Materials Letters 303 (2021) 130481

Contents lists available at ScienceDirect

Materials Letters

journal homepage: www.elsevier.com/locate/matlet

# The formation of B2-precipitate and its effect on grain growth behavior in aluminum-containing CoCrNi medium-entropy alloy

Hyomin Kim [a], Donghee Lee [b], Hyungjun Kim [c], Yejin Kim [c], Myeonghyeon Jang [c], Dongyoung Kwen [c], Yoonseong Koo [c], Eunjin Kim [c], Hyeonseok Cho [c], Maya Putri Agustianingrum [c,*], Nokeun Park [c,d,*], Boris Straumal [e,f,g,*]

[a] School of Advanced Root Industry Engineering, Yeungnam University, 280 Daehak-ro, Gyeongbuk 38541, Republic of Korea
[b] School of Materials Science and Engineering, Kyungpook National University, Daegu 41566, Republic of Korea
[c] School of Materials Science and Engineering, Yeungnam University, 280 Daehak-ro, Gyeongbuk 38541, Republic of Korea
[d] Institute of Materials Technology, Yeungnam University, 280 Daehak-ro, Gyeongsan, Gyeongbuk 38541, Republic of Korea
[e] Institute of Solid State Physics and Chernogolvka Scientific Center, Russian Academy of Sciences, Chernogolovka 142432, Russia
[f] National University of Science and Technology «MISIS», Moscow 119049, Russia
[g] Karlsruhe Institute of Technology, Institute of Nanotechnology, Eggenstein-Leopoldshafen 76344, Germany

ARTICLE INFO

*Keywords:*
Metals and alloys
Grain growth
Interfaces
Electron microscopy
B2-precipitate

ABSTRACT

B2-precipitate formation in $Al_{7.45}(CoCrNi)_{92.55}$ (at.%) was investigated after two-stage annealing. Prior face-centered cubic (FCC) grain growth has been successfully controlled using the pinning effect of B2-precipitate. Electron backscattered diffraction analysis was utilized to study the preferential growth direction of B2-precipitate during the second-annealing process. B2-precipitate as the partially coherent particle, exhibited Kurjumov-Sachs orientation relationship (OR) with FCC matrix in $\{111\}_{FCC}//\{110\}_{B2}$ plane and $\langle 110\rangle_{FCC}//\langle 111\rangle_{B2}$ direction. This orientation relationship altered the interface of B2-precipitate and FCC grain. The matched OR between B2-precipitate and FCC grain was effectively hindered the grain growth of FCC grain by giving the Zener pinning pressure.

## 1. Introduction

At room temperature, face-centered cubic (FCC)-based medium-entropy alloy (MEA) and high-entropy alloy (HEA) exhibit excellent plasticity while its strength can be improved through further strengthening by element addition and appropriate thermo-mechanical processing [1,2]. A cost-effective approach is obtained by minor solute addition to an equiatomic base of HEA and MEA systems. The addition of Al is not only cost-effective but also useful to reduce the specific weight of the alloy by increasing the Al content. Moreover, the negative mixing enthalpy between Al and other constituent elements in the HEA system leads to the formation of B2-precipitates [3]. The typical B2-precipitates in the HEA system have been explored as the coherent precipitates in the BCC matrix [4,5]. However, the combination of B2-precipitates and BCC matrix leads to brittleness instead of increasing strength. Therefore, it is preferable to utilize B2-precipitates in the FCC matrix since they can maintain the thermal stability of FCC structure at high-temperature. In the present work, an approach of two-stage annealing was applied to an equiatomic $Al_{7.45}(CoCrNi)_{92.55}$ (at.%). This Al content is adequate to introduce the precipitate formation along the grain boundaries (GBs) of $Al_{7.45}(CoCrNi)_{92.55}$ [6]. The precipitate formation and precipitate pinning-effect with the increasing of annealing temperature were carefully investigated. Then, various B2-precipitate morphologies, which are closely related to the crystal relationship between B2-precipitate and FCC matrix was analyzed.

## 2. Materials and methods

An alloy with a nominal composition of $Al_{7.45}(CoCrNi)_{92.55}$ (at.%) was fabricated using an arc-melting furnace in argon atmosphere using metal elements (purity > 99.9 at.%). The ingot was flipped about five times and then furnace-cooled in a copper mold. The as-cast alloy was homogenized at 1100 °C for 24 h. Subsequently, the specimen was cold-rolled with a total thickness reduction of 90%. The alloy was annealed at

* Corresponding authors at: School of Materials Science and Engineering, Yeungnam University, 280 Daehak-ro, Gyeongbuk 38541, Republic of Korea (N. Park). Institute of Solid State Physics and Chernogolvka Scientific Center, Russian Academy of Sciences, Chernogolovka 142432, Russia (B. Straumal).
*E-mail addresses:* mayaputri@ynu.ac.kr (M.P. Agustianingrum), nokeun_park@yu.ac.kr (N. Park), straumal@issp.ac.ru (B. Straumal).

https://doi.org/10.1016/j.matlet.2021.130481
Received 1 June 2021; Received in revised form 2 July 2021; Accepted 15 July 2021
Available online 17 July 2021
0167-577X/

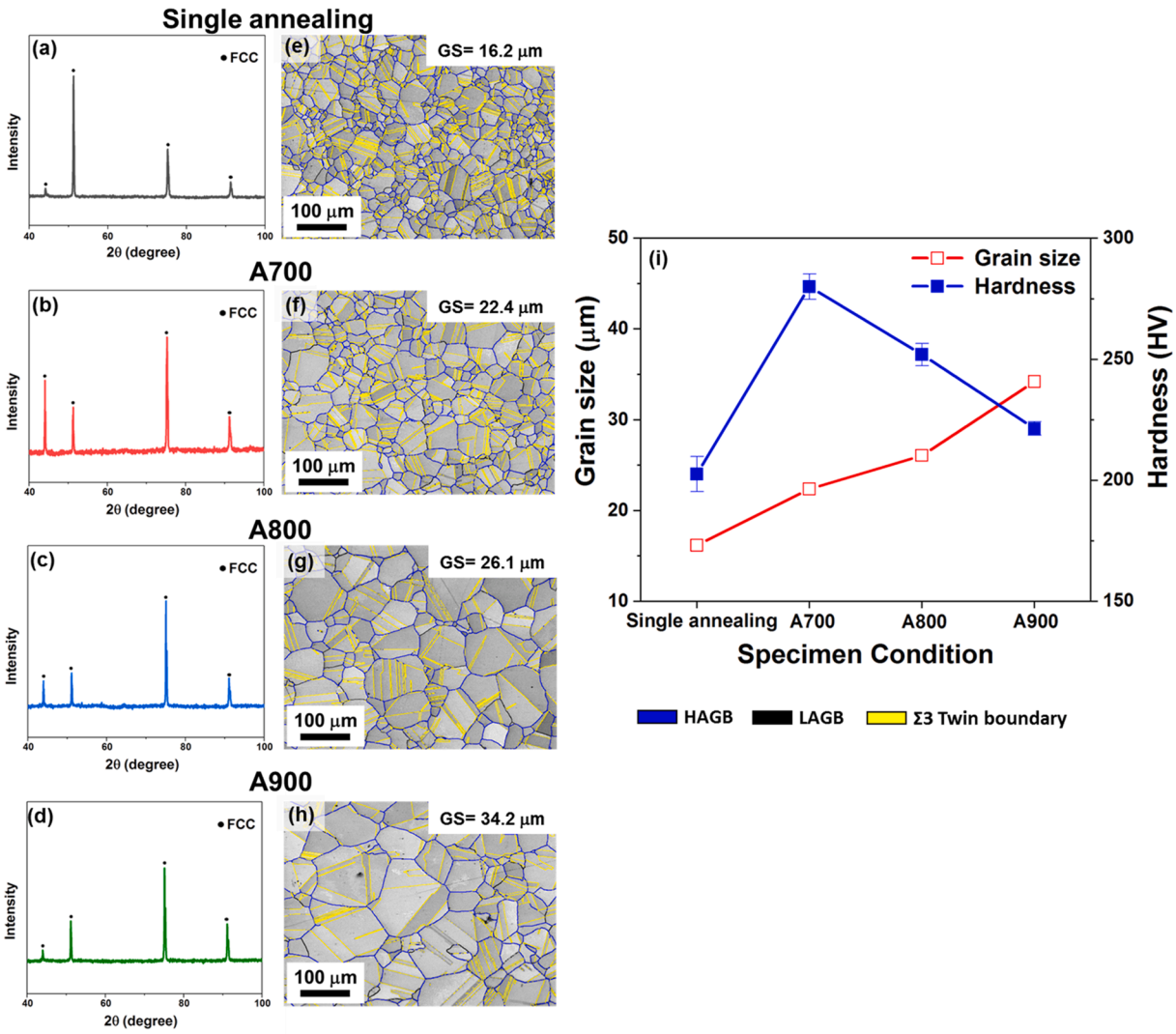


**Fig. 1.** (a–d) XRD Patterns and (e–h) SEM images after single-annealing 1100 °C and second-annealing at 700, 800, and 900 °C for 10 h, respectively. (i) Grain size and hardness as the function of different heat treatment conditions.

1100 °C for 5 min and followed by water quenching to obtain the recrystallized structure with a single-phase. The following heat treatment process was carried out at 700, 800, and 900 °C for 10 h (denoted as A700, A800, and A900, respectively) to promote the second-phase inside the alloy.

Mechanical properties were measured by Vickers microhardness tester. The initial phase identification was conducted using X-ray diffraction (XRD). Considering the relatively low accuracy of XRD to distinguish the precipitate, microstructure identification was precisely observed using a scanning electron microscope (SEM) in electron backscattered diffraction (EBSD) mode. The SEM-EBSD observation was performed to obtain the detailed microstructure, while the crystal orientation-relationship (OR) of the specimens was analyzed using TSL Orientation Image Microscopy (OIM) analysis software without applying clean-up procedure.

## 3. Results and discussion

XRD patterns and low-magnification SEM images of $Al_{7.45}(CoCrNi)_{92.55}$ for different heat treatment conditions are presented in Fig. 1. After single-annealing at 1100 °C, the peaks in XRD pattern (Fig. 1**a**) consisted of a single FCC phase. The corresponding SEM image in Fig. 1**e** showed that the single-annealing specimen had fully recrystallized grains with an average grain size of approximately 16.2 μm. The XRD pattern (Fig. 1**b–d**) and the microstructure (Fig. 1**f–h**) after second-annealing confirmed that the alloys still retained the FCC phase with the coarse recrystallized-grains. This result suggests that grain coarsening during the second-annealing process might be related to GB migration. Meanwhile, the second-phase was not visible in XRD patterns which might be due to the small size of precipitates.

The grain size and hardness of $Al_{7.45}(CoCrNi)_{92.55}$ were plotted as the function of different heat treatment conditions in Fig. 1**i**. It was observed that the grain size of the alloy (red) increased with increasing second-annealing temperature. Unlike the grain size's tendency, the hardness result (blue) showed a significant increase after second-annealing at 700 °C despite A700 grain size was coarser than a single-annealing specimen. This unusual hardness behavior after second-annealing can be explained by strengthening mechanism competition from Hall-Petch strengthening, solid-solution strengthening, and precipitation strengthening. In Hall-Petch strengthening, the dislocation glide is prevented by GBs. When the grain size increases, the "pure" Hall-Petch effect should lead to monotonous softening. The Hall-Petch strengthening can also compete with solid-solution strengthening. In solid-solution strengthening, material softening can also be occurred like the previous work in Al-15 wt% Zn alloy [7], complete decomposition of solid-solution phase led to the overall softening of material. Meanwhile, the softening from the solid-solution of Al in $Al_{7.45}(CoCrNi)_{92.55}$ can be neglected since the role of B2-precipitates in $Al_{7.45}(CoCrNi)_{92.55}$ is very significant [8]. In

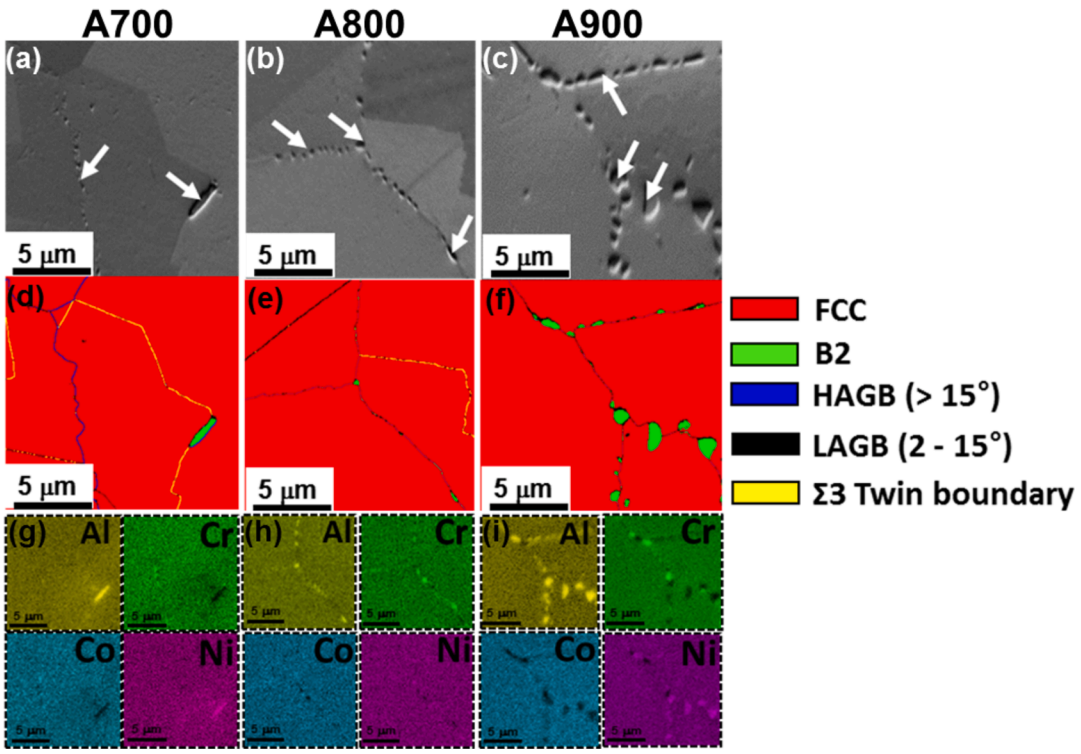


**Fig. 2.** High magnification SEM-BSE images (a–c), phase maps (d–f) and elemental distribution maps (g–i) of A700, A800, and A900, respectively. Precipitates are indicated by white arrows.

precipitation strengthening, the precipitates induce strains in the surrounding matrix and hinder dislocation. In the present work, the single-annealing alloy was free from precipitates. However, after secondary-annealing at 700 °C, the high magnification SEM-EBSD image in Fig. 2**a–c** displayed the precipitate along GBs and at GB triple junctions, which effectively prevented the dislocation glide and overcame the Hall-Petch softening. The phase maps in Fig. 2**d–f** indicated that the precipitate formation was dominated by B2 structure [9,10], which were enriched with Al and Ni (Fig. 2**g–i**). After secondary annealing at 800 and 900 °C, the B2-precipitates were larger and less coherent. This fact might also be linked to the role of B2-precipitate on retarding the moving GB using pinning effect [11]. The pinning mechanism might be affected by the variation of B2-precipitate/matrix crystal OR and the shape of B2-precipitate at GBs.

The representative images of A900 microstructure in Fig. 3**a** and **b** were selected to observe three different shapes of B2-precipitates. First, precipitate 1 in Fig. 3 exhibited a plate-like morphology. The OR of precipitate 1/FCC grain in G1 was not overlapped to each other, which indicated the interface was completely incoherent. Meanwhile, precipitate 1/FCC grain interface in G2 was coherent and shared the Kurdjumov–Sachs (K–S) OR at $\{1\,1\,1\}_{FCC}//\{1\,1\,0\}_{B2}$ plane and $\langle 1\,1\,0\rangle_{FCC}//\langle 1\,1\,1\rangle_{B2}$ direction. Precipitate 2 in Fig. 3 which was located at the triple junction of FCC grain had a rounded morphology. The detailed OR analysis confirmed that B2-precipitate at this area had a partially coherent interface with the FCC grain. The corresponding OR analysis at G3 and G4 revealed that they shared the K–S OR, however G5 had incoherent interface which made G5 was curved into grain interior [12,13]. Precipitate 3 in Fig. 3 represented the B2-precipitate between two adjacent grains which had a rounded morphology. The precipitate 3/FCC grain interface obviously showed the GB wetting phenomenon [14] during grain growth. The corresponding OR analyses from precipitate 3 in pole figures G6 and G7 described the incomplete wetting of GB by B2-precipitate. The interface at G6 exhibited a smaller wetting angle at GB, which was confirmed by the overlapped planes and direction poles. Meanwhile, the high interfacial anisotropy, which was shown by the B2-precipitate and FCC grain at G7, resulting in B2-precipitate grew straightly into the grain interior of G7. Based on these analyses, B2-precipitate in $Al_{7.45}(CoCrNi)_{92.55}$ mostly exhibited a partially coherent precipitate.

The role of B2-precipitates during the grain growth in $Al_{7.45}(CoCrNi)_{92.55}$ can be described quantitatively by the Zener pinning effect. As has been mentioned by Zener [15], the pinning pressure from the particle at the boundary of two-phase alloys which homogeneously distributed can be expressed as:

$$P_Z = \frac{3\gamma F_V}{d} \tag{1}$$

where γ is boundary surface energy and $F_V$ and $d$ are fractions and average sizes of dispersed precipitates. Since the B2-precipitates were dispersed at GBs, the pinning pressure on boundary ($P_B$) is affected by its particle size and volume fraction, and it can be estimated as:

$$P_B = \frac{\gamma F_{vB} D}{d^2} \tag{2}$$

where $F_{vB}$ is the fraction of particles located at the boundaries, and $D$ is the grain size. The value of γ was obtained from NiAl-based B2-precipitate [16]. Based on **Eq. (2)**, the pinning pressure decreased with the increase of second-annealing temperature (see Table 1). Here, the size stability of the B2-precipitate provided a significant contribution to the pinning pressure. The highest pinning pressure was obtained by A700 since it had the smallest precipitate size. Meanwhile, B2-precipitate in A900 gave a minor contribution to the pinning pressure due to the coarse precipitate size despite the high volume fraction.

## 4. Conclusion

B2-precipitates were introduced at GBs of recrystallized-$Al_{7.45}(CoCrNi)_{92.55}$ via cold-rolling and multi-stage heat treatment. The role of B2-precipitate during grain growth was successfully investigated, and the following conclusions were drawn.

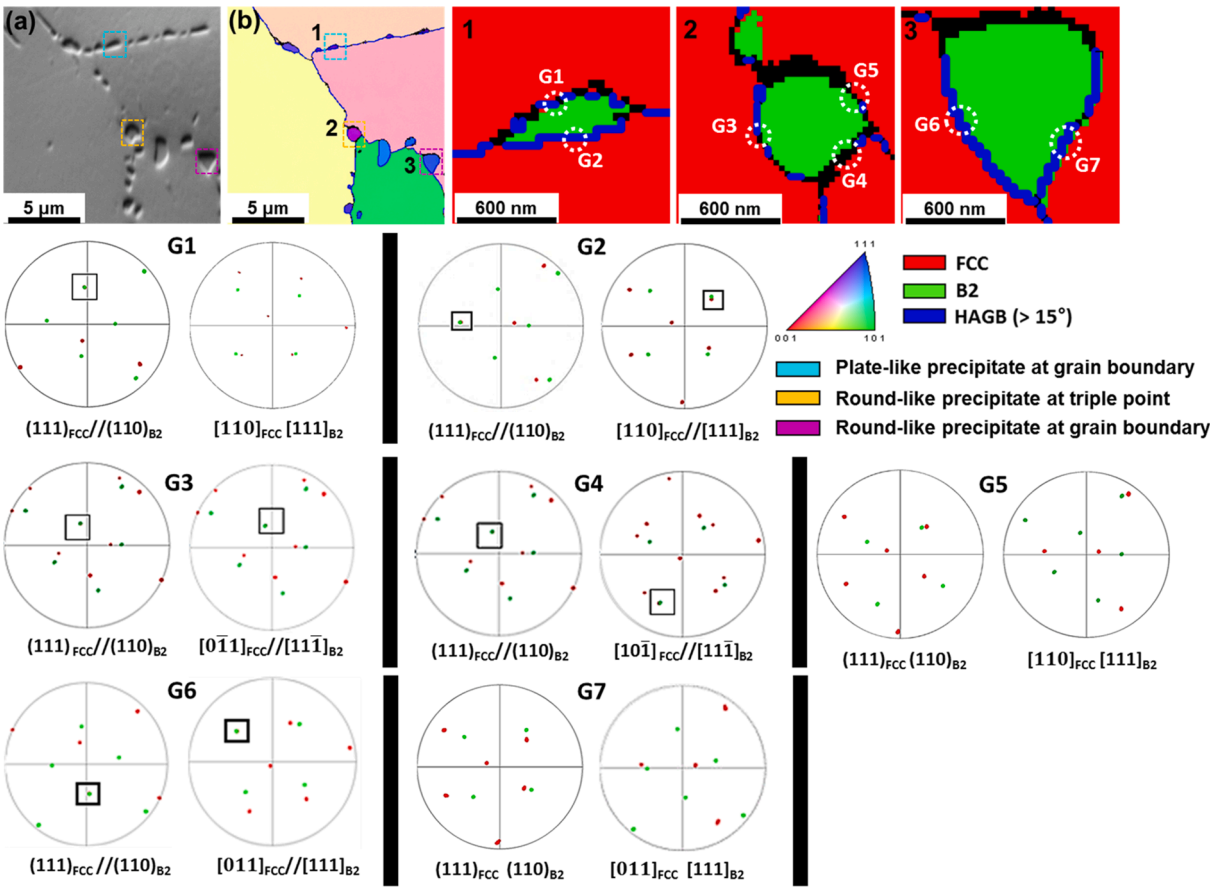


**Fig. 3.** (a) Representative high magnification SEM-BSE image with (b) corresponding IPF map of A900 shows coarse precipitates with different morphologies. The dotted squares in (a) indicate the representative precipitates (1, 2, and 3) with corresponding OR direction and plane pole figures between FCC matrix and B2-precipitate. The overlapped poles are indicated with black rectangles. The black points surrounding the precipitate area in 1, 2, and 3 denote zero solution data points.

**Table 1**
B2-precipitate parameters after second-annealing for 10 h.

| Temperature (°C) | Volume Fraction, $F_{vB}$ | Diameter of precipitate, $d$ (μm) | Pinning pressure, $P_B$ (MPa) |
|---|---|---|---|
| 700 | 0.0040 | 0.0610 | 6.0092 |
| 800 | 0.0012 | 0.0760 | 1.3540 |
| 900 | 0.0130 | 1.8600 | 0.0321 |

- Despite the grain coarsening, the significant hardness increment in A700 demonstrated the significant role of precipitation strengthening.
- The B2-precipitate at GBs exhibited the partially coherent precipitate in $Al_{7.45}(CoCrNi)_{92.55}$, which still effectively pinned the grain growth.
- The quantification of pinning pressure at boundaries by Zener's model estimated that A700 had the highest pinning pressure than A800 and A900 with precipitate size highly determined the pinning-effect at GBs.

## CRediT authorship contribution statement

**Hyomin Kim:** Conceptualization, Methodology, Writing - original draft. **Donghee Lee:** Investigation, Visualization. **Hyungjun Kim:** Investigation, Methodology. **Yejin Kim:** Investigation, Methodology. **Myeonghyeon Jang:** Investigation, Methodology. **Dongyoung Kwen:** Investigation, Visualization. **Yoonseong Koo:** Investigation, Methodology. **Eunjin Kim:** Investigation, Methodology. **Hyeonseok Cho:** Investigation, Visualization. **Maya Putri Agustianingrum:** Resources, Writing - original draft, Writing - review & editing. **Nokeun Park:** Conceptualization, Validation, Supervision. **Boris Straumal:** Validation, Writing - review & editing, Supervision.

## Declaration of Competing Interest

The authors declare that they have no known competing financial interests or personal relationships that could have appeared to influence the work reported in this paper.

## Acknowledgment

This work was supported by the 2021 Yeungnam University Research Grant.

## References

[1] M.P. Agustianingrum, S. Yoshida, N. Tsuji, N. Park, J. Alloys Compd. 781 (2019) 866–872.
[2] D. Lee, M.P. Agustianingrum, N. Park, N. Tsuji, J. Alloys Compd. 800 (2019) 372–378.
[3] T.T. Shun, C.H. Hung, C.F. Lee, J. Alloys Compd. 493 (2010) 105–109.
[4] M. Feuerbacher, Sci. Rep. 6 (2016) 29700.
[5] L.J. Zhang, K. Guo, H. Tang, M.D. Zhang, J.T. Fan, P. Cui, Y.M. Ma, P.F. Yu, G. Li, Mater. Sci. Eng. A 757 (2019) 160–171.
[6] D. Lee, H.U. Jeong, K.H. Lee, J.B. Jeon, N. Park, Mater. Lett. 250 (2019) 127–130.
[7] A.A. Mazilkin, B.B. Straumal, M.V. Borodachenkova, R.Z. Valiev, O.A. Kogtenkova, B. Baretzky, Mater. Lett. 84 (2012) 63–65.
[8] B. Gwalani, V. Soni, D. Choudhuri, M. Lee, J.Y. Hwang, S.J. Nam, H. Ryu, S. H. Hong, R. Banerjee, Scr. Mater. 123 (2016) 130–134.

[9] M.H. Tsai, K.Y. Tsai, C.W. Tsai, C. Lee, C.C. Juan, J.W. Yeh, Mater. Res. Lett. 1 (2013) 207–212.
[10] P. Sathiyamoorthi, J.W. Bae, P. Asghari-Rad, J.M. Park, J.G. Kim, H.S. Kim, Entropy 20 (2018) 1–11.
[11] D.E. Jodi, J.H. Park, N. Park, Mater. Charact. 157 (2019), 109888.
[12] K. Huang, K. Marthinsen, Q. Zhao, R.E. Logé, Prog. Mater. Sci. 92 (2018) 284–359.
[13] E. Nes, N. Ryum, O. Hunderi, Acta Mater. 33 (1985) 11–22.
[14] A.B. Straumal, B.S. Bokstein, A.L. Petelin, B.B. Straumal, B. Baretzky, A.O. Rodin, A.N. Nekrasov, J. Mater. Sci. 47 (2012) 8336–8343.
[15] T. Nishizawa, I. Ohnuma, K. Ishida, Mater. Trans. JIM 38 (1997) 950–956.
[16] T. Hong, A.J. Freeman, Phys. Rev. B 43 (1991) 6446–6458.